David C. Goodrich
Department of Civil and Environmental Engineering
University of Wisconsin
Madison, WI 53706

A Simple 35-mm SLR Photogrammetric System for Glacier Measurements*

Field procedures, camera calibration, system testing, and the use of the parallax equations and a parallax correction graph are described.

Introduction

In 1976 a study in the Sir Sanford Range of the Selkirk Mountains in British Columbia was initiated to collect basic data in this remote, uninvestigated area. A major objective of this research expedition was to define glacier terminus locations and to monitor their movements on a periodic basis. Two glaciers in the area were dangerous to approach for this work because of crevasses and possible avalanches. Thus, a data collection problem existed in which the application of terrestrial photogrammetry could be used as a solution.

Because of the ever changing nature of glaciers, it was decided that an accuracy to within the nearest foot for the location and shape of the glacier snout would be sufficient. Several externally imposed limitations existed in this study, which suggested the use of a system employing a small non-metric camera. Two of these limitations were

- Weight and size limitations in transporting equipment in remote and rugged terrain, and
- The high cost of precise photogrammetric equipment and limited access to it.

With these limitations and relatively low order accuracy requirements, it was hypothesized that a 35-mm single lens reflex (SLR) camera and analysis using a parallax bar would perform adequately. Tests discussed in this paper illustrated that these accuracies can be achieved to object distances of 110 feet.

Abstract: *The uses of terrestrial photogrammetry are becoming more diverse and widespread. Further expansion of its application would likely occur if associated costs could be reduced. If the required accuracies of a project are not of high order, this cost reduction can be achieved using a 35-mm single lens reflex (SLR) camera system. This paper discusses a simple system which utilizes SLR photos with a stereoscope and parallax bar. Tests using the system showed that desired accuracies for glacier measurements could be achieved. This system can be employed by anyone having the elementary equipment and a basic knowledge of terrestrial photogrammetry.*

Field Procedure

Formulation of field procedures considered the above constraints as well as additional difficulties which arose upon detailed examination of the problem. Because of the dangerous nature of the glacier, targets for control could not be placed on the glacier. Controlling the stereopair by enforcing the omega, phi, and kappa orientation angles equal to zero was impractical and nearly impossible in the uneven and rugged terrain. Instead, it was decided to select distinct control points on the glacier itself. These points were selected in locations as near as possible to the classic photo-control point locations. The X, Y, and Z coordinates of these photo-control points were then established by a two-station space intersection. Be-

* Revised version of the paper for which the author received the 1980 Bausch and Lomb Award, Undergraduate Division.

Photogrammetric Engineering and Remote Sensing,
Vol. 48, No. 9, September 1982, pp. 1477-1485.

0099-1112/82/4809-1477$02.25/0

cause the points selected were not easily identifiable (i.e., targeted), a picture of the glacier was taken with a polaroid type camera and the photocontrol was identified and marked directly on this photo. These points could then be identified on an enlarged 35-mm negative during orientation. The safety of the survey party from glacial mishaps was, therefore, assured because no direct contact with the glacier was required.

A summary of the field procedures employing the above technique follows (see Figure 1):

(1) Perform a preliminary (rough) stadia survey to ensure proper base/depth and elevation requirements.
(2) Lay out the camera baseline and establish and identify permanent camera stations that may be recovered for future use.
(3) Select photo-control by looking through the camera itself, holding it level and roughly perpendicular to the baseline.
(4) Photograph the photo-control with a polaroid type camera from each camera station; mark and identify the photo-control on these photos (see Figure 2).
(5) Set up the theodolite over each camera station and turn horizontal and vertical angles to the photo-control points.
(6) Turn a 90° angle with the theodolite from the other camera station and sight some recognizable "alignment point" on the line of sight.
(7) Using a special camera tripod adapter, set the camera over the camera station, level it so that omega and phi are equal to zero, and record the height above ground of the camera.
(8) Sight the "alignment point" located on a perpendicular line from the baseline to insure that kappa equals approximately zero. This is accomplished by centering the "alignment point," selected in step six, by eye in the field-of-view of the 35-mm SLR camera.
(9) Expose several photographs with a range of exposure settings (focal length set to infinity).
(10) Repeat steps four through nine while working over the other camera station.

The camera used in the above procedure was a 35-mm SLR Olympus OM-1 with nominal 50-mm focal length. The camera tripod adapter allowed attachment of the camera to the tripod and enabled leveling and centering of the camera. Because the exact location of the rear nodal point of the camera was unknown at the time, the exact coordinates of the nodal point may be offset slightly from the X, Y coordinates of the camera station. However, if the camera is set up via step 7 in the field procedures, the adapter does provide a reproducible spatial location of the nodal point with respect to the camera station. If necessary, this constant error can be accounted for. For purposes of this study, the maximum estimated offset of approximately 0.05 ft was considered negligible.

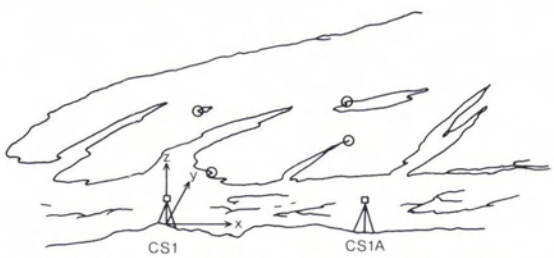

FIG. 1. Camera station baseline in front of glacier.

FIG. 2. Polaroid photo of glacier with photocontrol points circled.

CAMERA CALIBRATION

The central component of this system, as with any photogrammetric system, is the camera. Expensive metric cameras are manufactured for stability and incorporate lenses with high geometric accuracy, with little or negligible principal point offset. A non-metric 35-mm SLR camera such as the one used in this project, on the other hand, is manufactured for pictorial quality and has a variable image distance. Thus, the first phase of the accuracy analysis involved determination of the calibrated focal length, principal point offset, and radial lens distortions of the camera.

Determination of the camera parameters for this project was accomplished using a previously developed camera calibration procedure (Wolf and Loomer, 1975). In this procedure, the first step involved photographing a camera calibration test field. The X, Y, and Z coordinates of the targets in the test field had been established by a precise photogrammetric surveying using a metric camera and a three-station simultaneous solution. The test field targets consisted of window corners on a large building. The targets were chosen to form a

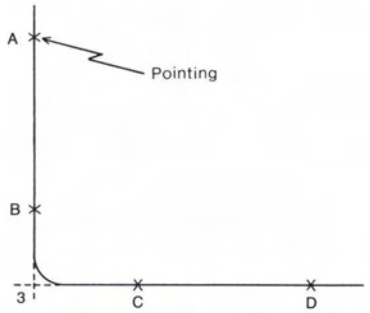

FIG. 3. Determination of corner fiducials.

large "×" shape centered across the diagonals of the camera format. In addition, approximate coordinates of the camera were measured at the time of exposure.

The second step of the calibration process consisted in measuring the photocoordinates of the exposed calibration photos. This was done using a Kern PG-2 stereoplotter (Wolf and Pearsall, 1976) interfaced with a H. Dell Foster Digitizer. The X, Y photocoordinates were referenced to an arbitrary measurement coordinate system and punched out on computer cards. The 35-mm SLR negative was placed very near the center cross of the plate carriers. This cross was used as the origin for the arbitrary monocomparator coordinate system in order to insure repeatability of initialization of the digitizer.

Three pointings were taken on each target point in order to increase accuracy and eliminate blunders. Pointings were also taken on the edges of each side of the format so that reproducible and distinct corner points of the rectangular format could be calculated and used as "fiducial marks" (see Figure 3). This was performed by calculating the intersection of the lines $\overline{AB}$ and $\overline{CD}$ locating fiducial point 3 (similarly for the remaining three corner marks).

At this point, coordinates of the fiducial marks are known in the arbitrary measurement system. These coordinates are used to compute lengths of the format sides x_b, x_t, y_ℓ, and y_r in Figure 4 from the equation

$$x_t = D_{12} = [(x_2 - x_1)^2 + (y_2 - y_1)^2]^{1/2}. \quad (1)$$

These distances are used to define coordinate constraints imposed upon the fiducial marks to form a principal point origin system (Figure 4). In this system the x and y axes are constrained to be parallel to the bottom and left edge of the format, respectively. With known fiducial mark coordinates in the measurement and principal point system, a transformation of the target points into the principal point system is possible. For this study an affine transformation was used. This also accounted for differential film shrinkage.

Output from the affine transformation provided photocoordinates of the targets in the fiducial axis system in millimetres. These coordinates were input into the camera calibration program. Additional input included the ground coordinates of the targets, ground coordinates of the camera station, and initial approximations of omega, phi, and kappa. Using a least-squares solution of a modified collinearity equation, the program computed the following camera parameters:

- Principal point offsets, x_0 and y_0;
- Calibrated focal length of the lens;
- Omega, phi, and kappa at the time of exposure; and
- The radial lens distortion coefficients k_1, k_2, k_3 and k_4 for the equation

$$d = k_1 r + k_2 r^3 + k_3 r^5 + k_4 r^7 \quad (2)$$

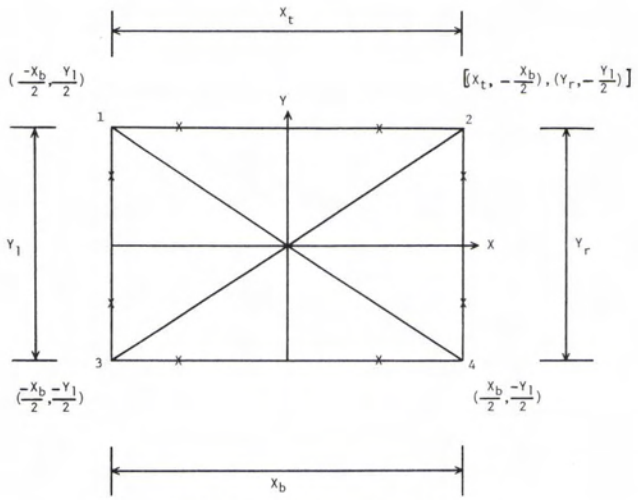

FIG. 4. Fiducial axis system.

where d = radial lens distortion in (mm) and
r = radial distance in (mm).

The overall radial lens distortions (see radial lens distortion curve, Figure 5) were small and well within the accuracies reported for the objectives of this study (the residuals on the majority of targets measured were below 20 micrometres, but some points had residuals in the 40 to 50 micrometre range). This problem could have been reduced if more pointings had been taken per point in order to obtain a more statistically significant average. The calibrated focal length (51.21 mm) was significantly different from the nominal 50-mm focal length stamped on the lens.

The principal point offsets were quite large ($x_0 = -0.251$, $y_0 = 0.359$ mm), but this may be expected, because accurate lens centering in the manufacture of most 35-mm SLR cameras is not of high priority. These effects can be accounted for in the photogrammetric solutions for coordinates. (However, the x_0 principal point offset cannot be accurately accounted for in aiming the camera in field procedure 7.)

Testing of the System

With the camera calibration completed, evaluation of the accuracy of the system as a whole was possible. Testing a stereopair of 35-mm photographs required the establishment of a three-dimensional target array. An array was established and photographed so as to obtain proper stereo coverage.

Site selection criteria for the target array was very similar to that described for the glacial photography. Proper overlap, maximum and minimum depths of field, and a proper base/depth ratio also had to be designed into the target array.

Detailed calculations to determine the proper size, shape, and locations of the target array to meet the project objectives was carried out. Several types of targets were selected to be used in the target array (see Figure 6). They included targets derived from the existing building (window corners) as well as artificial targets comprised of 2-inch diameter styrofoam balls suspended along a wire, and targets mounted on tripods (see Figure 7).

The camera stations were laid out in advance of the target array and their relative locations were determined. Two camera baselines were established in order to see how the distance to the targets affected the accuracy. Baseline lengths of 31.695 ft and 63.485 ft were used, corresponding to nominal 100 ft and 200 ft distances, respectively. This yielded a base/height ratio of approximately 0.32. This relatively small base/height ratio was necessary to achieve 55 percent overlap because of camera format and focal length constraints. The ground coordinate system was defined with its origin at **CS1** and the X axis passing through **CS1A** (see Figure 1).

Ground coordinates of the targets were determined by field survey, and they were also computed photogrammetrically and compared with the known ground coordinates.

Photograph Analysis Using Parallax Equations and a Parallax Correction Graph

As noted earlier, low order accuracy requirements prompted the decision to use parallax equations to analyze the stereopairs. The mea-

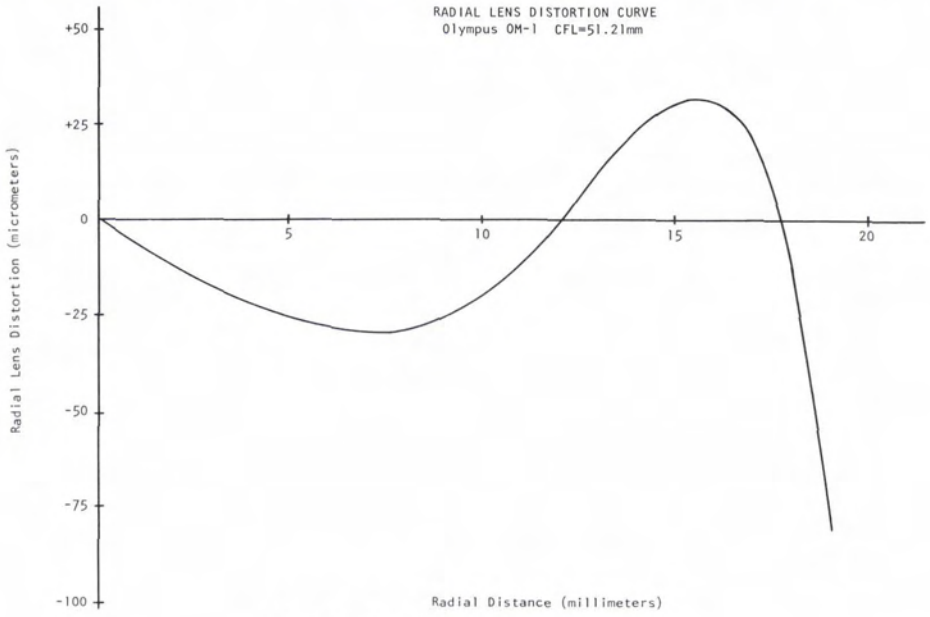

Fig. 5. Radial lens distortion curve.

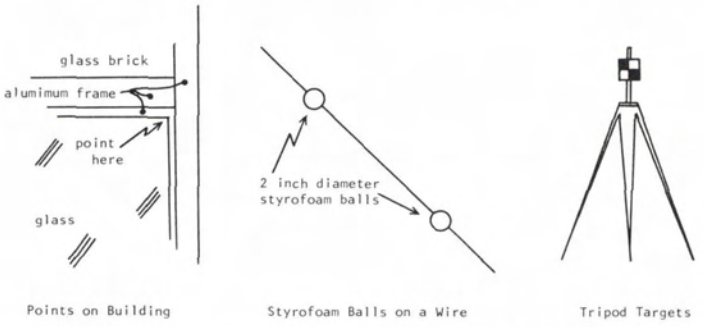

FIG. 6. Types of targets employed.

sured parallax from a parallax bar used in these equations inherently contains various errors that cannot be directly accounted for. To help compensate for these errors a parallax correction graph (Wolf, 1974, pp. 162–164) was used. This simple nomographic technique of analysis employs relatively simple equipment and, hence, is economical from a hardware viewpoint. In this method six control points *well distributed* in the stereo-overlap area were selected to construct the correction graph. From the known coordinates, the theoretically correct parallax of point a could be computed by

$$P_{T_a} = \frac{Bf}{Y_a} \tag{3}$$

The baseline distance, B, was measured as a part of the control survey, and the camera focal length was computed by multiplying the enlargement ratios of the paper prints used by the calibrated focal length.

FIG. 7. Side view of target array.

The theoretically correct parallax values were then compared to the measured parallax values and the differences were computed. A transparent overlay was then placed over the overlap area of the stereopair and the control point locations were accurately marked on it. Using the computed parallax differences, points of equal parallax correction were connected by isolines in the same fashion that contours of equal elevation would be constructed on a map (see Figure 8).

By overlaying the parallax correction graph on the overlap area of the photograph, a parallax correction was obtained for each of the points whose parallaxes had been measured. The correction was then applied to the measured parallax, and this corrected parallax was used to compute coordinates by using the following terrestrial photogrammetric parallax equations:

$$Y_a = \frac{Bf}{P_{c_a}} \tag{4}$$

$$X_a = \frac{Bx_a}{P_{c_a}} \tag{5}$$

$$Z_a = \frac{By_a}{P_{c_a}} \tag{6}$$

P_c = corrected parallax

In this study the negative stereopairs of the target array were enlarged approximately 6.7 times on paper prints. Care was taken in enlarging the negatives to insure parallelism between negative and enlargement planes so that distortions were not introduced.

The average enlargement ratio from the stereopair was applied to the calibrated focal length and principal point offset distances. Photo-coordinate axes were laid out on the enlarged prints by simply finding the midpoint of the left and bottom sides of the format. As mentioned earlier, the principal point offsets obtained in camera calibration were quite large. Therefore, both the enlarged x_0 and y_0 principal point offset distances were applied to all measured photo-coordinates before they were used in Equations 5 and 6. Photo-coordinates x and y were measured for all targeted points of the test range. With the

photo-coordinates measured, the stereopair was setup on a rigid matte board for stereoviewing in such a manner as to account for unequal camera station elevations so that Equations 4 through 6 could be used without modification (Wolf, 1974, pp. 407–408).

Using an ordinary stereoscope and parallax bar, the parallaxes of all control points in the test range were measured. These parallaxes were used to compute the X, Y, Z coordinates of the control points without modification and compared to the coordinates computed with parallaxes corrected by the parallax correction graph.

The following example, using the 100 ft nominal distance stereopair, will help illustrate the method described above. Six control points, uniformly distributed in the stereo-overlap area, were chosen as "control points" for constructing the parallax correction graph (see Table 1). Parallax of the control points was measured on the stereopairs and was computed from ground coordinates. The parallax correction in column #5 of Table 1 was calculated by subtracting the measured parallax from the computed parallax. These values were used to construct the parallax correction graph shown in Figure 8.

Seven of fourteen other points of known ground coordinates used in the 100 ft photographs are also shown in Figure 8. From this figure, parallax corrections were interpolated for the non-control points and applied to their measured parallaxes. The corrected parallaxes were then used to compute X, Y, and Z ground coordinates for the non-control points (Table 2).

Uncorrected parallaxes were also used to compute ground coordinates of the targets to form a basis for comparison. For calculation of coordinates using both uncorrected and corrected parallaxes, the differences from the true value

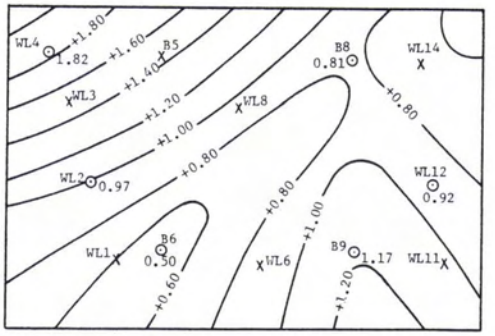

FIG. 8. Parallax correction graph for photos #4 and #9.

obtained by ground survey were computed. The applicable equations are

$$X_D = X_C - X_G \tag{7}$$

$$Y_D = Y_C - Y_G \tag{8}$$

$$Z_D = Z_C - Z_G \tag{9}$$

In Equations 7, 8, and 9, X_D, Y_D, and Z_D are discrepancies, and the subscripts C and G refer to computed coordinates and ground surveyed coordinates, respectively. The mean, standard deviation, s, and variance, s^2, for Y_D, X_D, and Z_D were computed from the tabulated target point list. In computing these values, all points in the target range were included when using measured parallax. Twenty and 63 targets existed in the stereo-overlap area for the 100 ft and 200 ft distance photopairs, respectively. When using the corrected parallax, the target points used to construct the parallax correction graph (six targets) were withheld when computing Y_D, X_D, and Z_D.

TABLE 1. CALCULATIONS TO SET UP PARALLAX CORRECTION GRAPH FOR PHOTOS #4 AND #9 MODIFIED METHOD VIA WOLF, (1974, pp. 162–163)

1 Control Point	2 Y Coor. Depth (ft)	3 Parallax Measured (mm) P_m	4 Parallax Calc. (mm) $P_G = \frac{Bf}{Y}$ *	5 $C_P = P_G - P_m$ (mm)
B6	1110.40	97.61	98.11	+0.50
WL2	1092.27	116.42	117.39	+0.97
WL4	1100.65	105.79	107.61	+1.82
B8	1110.39	97.31	98.12	+0.81
WL12	1088.43	121.57	122.49	+0.92
B9	1110.41	96.93	98.10	+1.17

* Note: Y used in Eq. in column 4 = Y (column 2) − 1000.00 (CS1 datum)
(a) $f = (f_{cal.})$ (enlargement ratio)
= (51.21 mm) (6.6734) = 341.74 mm
(b) B = 31.695 ft
(c) P_G = parallax computed from surveyed ground coordinates

TABLE 2. GROUND COORDINATES FROM CORRECTED PARALLAX PHOTOGRAPH #4 AND #9, NOMINAL DISTANCE 100 FT.

Point	Measured (P_m) mm	Parallax Correction (from graph) (C_P) mm	Corrected Parallax $P_c = P_m + C_P$ mm	$Y = Y_s + \frac{Bf}{P_c}$ ft	$X = X_s + \frac{Bx}{P_c}$ ft	$Z = Z_s + \frac{By}{P_c}$ ft
B5	97.22	1.44	98.66	1109.79	1012.82	1024.24
WL1	123.55	0.60	124.15	1087.25	1007.35	1006.74
WL3	110.11	1.47	111.58	1097.07	1004.40	1018.85
WL6	129.92	0.86	130.78	1083.86	1016.01	1006.48
WL8	114.04	0.93	115.00	1094.19	1016.55	1018.04
WL11	129.84	1.03	130.87	1082.77	1027.45	1006.66
WL14	109.13	0.69	109.82	1103.62	1030.89	1027.06

X_s, Y_s, Z_s = Camera Station Coordinates (1000.00, 1000.00, 1000.00).
Note: Y in the terrestrial case equals Z in the aerial case.

RESULTS

The results of the comparison when using uncorrected versus corrected parallaxes indicate that a major improvement in the number of points falling within the desired accuracy limits of within one foot was achieved. These results are tabulated in Table 3.

The results indicate that the system developed can be used in conjunction with analysis by a parallax correction graph to nominal distances up to 100 feet. Distances of targets used in the 100 foot nominal test stereopair ranged from 87 to 111 feet. In the nominal 100-foot test the corrected parallax was used to compute all coordinates.

In the 200-foot nominal-test stereopair, large systematic discrepancies existed in the measured parallax values and could not be entirely corrected for when using the parallax correction graph. Unlike the 100-foot test, the same corrected parallax could not be used to correct measured parallaxes for all three coordinates. A separate parallax correction graph was constructed for Y coordinates using Equation 3 and for X coordinates using

$$P_{T_a} = \frac{Bx_a}{X_a} . \tag{10}$$

All Z coordinates fell within the specified accuracy limits, so a separate graph was not constructed to adjust these values. It is recommended that, for distances greater than 100 feet, a separate parallax correction graph be constructed for each coordinate.

Non-perpendicularity of the camera axes to the camera station baseline is thought to be the cause for the degradation in accuracy at greater distances. Because the system developed does not allow for a direct accurate measure of the camera axis direction from the baseline, errors due to this faulty alignment would be magnified at greater distances. The large X_0 principal offset distance would also contribute to this error as it cannot be compensated for when aligning the camera by eye

TABLE 3. SUMMARY OF RESULTS

Photos	Nominal Depth	Method	Y_D Statistics	X_D Statistics	Z_D Statistics	$\%Y_D \leq \pm 1$ ft	$\%X_D \leq \pm 1$ ft	$\%Z_D \leq \pm 1$ ft
4 & 9	100 ft	Using Uncorrected Parallax	$\bar{Y}_D = +0.86$ $s = 0.46$ $s^2 = 0.21$	$\bar{X}_D = +0.48$ $s = 0.14$ $s^2 = 0.018$	$\bar{Z}_D = +0.32$ $s = 0.13$ $s^2 = 0.016$	65	100	100
4 & 9	100 ft	Using Corrected Parallax	$\bar{Y}_D = -0.07$ $s = +0.48$ $s^2 = 0.23$	$\bar{X}_D = +0.32$ $s = 0.11$ $s^2 = 0.012$	$\bar{Z}_D = +0.19$ $s = 0.058$ $s^2 = 0.003$	100	100	100
21 & 14	200 ft	Using Uncorrected Parallax	$\bar{Y}_D = +5.55$ $s = 1.17$ $s^2 = 1.37$	$\bar{X}_D = +0.73$ $s = 0.55$ $s^2 = 0.55$	$\bar{Z}_D = +0.057$ $s = 0.42$ $s^2 = 0.18$	0	68	100
21 & 14	200 ft	Using Corrected Parallax	$\bar{Y}_D = -0.69$ $s = 0.54$ $s^2 = 0.29$	$\bar{X}_D = +0.26$* $s = 0.32$ $s^2 = 0.10$	$\bar{Z}_D = +0.06$ $s = 0.42$ $s^2 = 0.18$	68	100	100

* A separate parallax correction graph was constructed for X coordinates using $P_{c_a} = (Bx_a/X_a)$; $\bar{X}_D$, $\bar{Y}_D$, $\bar{Z}_D$ equal the mean discrepancies
s equals standard deviation
s^2 equals variance

(field procedure, step 7). The alignment error is readily apparent from examination of the Y coordinates computed from the 200-foot test photographs. The non-perpendicularity shows in Y coordinates because it produces a consistently high value (>90° angle to baseline). The magnitude of the discrepancies (Y_D) is greater than X_D or Z_D because of the weak intersection angle obtained to calculate the Y coordinates.

Examination of the x-parallax correction graph for the 200-foot test shows that discrepancies vary in almost a linear fashion as the x photo-coordinate increases. This would indicate that, as the angle from the camera axis increases, the errors introduced by non-perpendicularity increase. This is consistent with terrestrial photogrammetric equations for non-perpendicular stereophotography. It is speculated that the z-coordinate computations were not highly affected by the non-perpendicularity because the vertical angles of all the targets were very small at the greater distance. Hence, the errors in the horizontal distance to the target point (inherent in the parallax) are multiplied by small values (inherent in the y photo-coordinate) to obtain the vertical offset needed to compute the Z ground coordinate.

Application to Glacier Measurements

The field procedures outlined earlier were used to obtain stereopairs along the snout areas of the Silvertip and Sir Sanford Glaciers. Because of the deterioration in accuracy at distances greater than 110 ft, the area of stereocoverage is limited. This is not entirely detrimental because most glacier snouts are curved, and several camera baselines must be established to encompass the snout.

Site selection of the photo baselines posed the greatest problem in measuring the glaciers. Because of the uneven and rugged nature of the terrain, considerable time was required to locate camera station points that satisfied stereocoverage constraints and provided a clear view of the glacier. The greatest limitation was the requirement to level the camera. This requirement could be eliminated by using analytic techniques, and this will be investigated. An analytic approach would also require more sophisticated equipment and photogrammetric knowledge. It should be stressed that the simplicity of the system discussed is its strength.

Weather and terrain conditions are major factors influencing the time required to obtain stereopairs. To obtain three stereopairs (from four camera stations), it is estimated that one to one-and-one-half days would be required by a two-person crew. This would include establishment and location of the camera stations, location and survey of photocontrol, and exposure of the photographs.

When laying out the camera stations, a significant recession or advance of the glaciers in the future was also considered. Such changes may force the relocation of camera stations in order to provide adequate stereocoverage. For this reason, control stations near the camera stations but far enough from the influences of the ice were also established when initial base mapping was performed. The Silvertip and Sir Sanford glaciers are relatively small valley glaciers, and the lower lobe of the snout was successfully measured by the procedure outlined. Problems would arise in applying this system to large ice masses.

For the glaciers studied, application of the parallax correction graph technique to the glacier photography was also readily accomplished. Using a parallax bar to analyze the photos has a distinct advantage over the use of most stereoplotters because a very large range in parallax can be accommodated. Also, fewer restrictions are imposed on control point location on the glacier.

Using control points, the same procedure discussed for parallax correction graph construction was used. From this, ground coordinates of points defining the location and shape of the glacier snout were computed. Some problem does exist in setting the floating mark of the parallax bar on the white and uniformly textured areas of the glacier. Fortunately, the majority of photos taken for this study were of glacier snouts with irregularities and which were soiled by moraine material.

Future Research Objectives

The test target array photographs were taken so that the following two methods can be used to determine ground target coordinates. These methods are

- Relative orientation on the Kern PG-2 accompanied by a three-dimensional transformation into the absolute coordinate system, and
- Fully analytical solution using the collinearity equations.

These methods of analysis could be used to determine the increase in accuracy, if any, that would be obtained by using these more elaborate methods. Costs and equipment availability must also be examined to determine which of the three methods will give the most suitable solution to a specific measurement problem from a cost/benefit point of view.

Work should also be directed toward improving the perpendicularity of the camera axis to the baseline. If this were accomplished, the simple low cost parallax correction graph method could be used in a wider range of applications.

Conclusions

The camera calibration procedure was easily performed and is well adapted to the calibration of a non-metric 35-mm SLR camera. The results indi-

cate that a 35-mm camera can be used in the system described for obtaining stereopairs without fear of significant distortion errors being introduced by the camera. Alignment errors when photographing the stereopairs appears to be the main cause of error.

The procedure described for obtaining the stereopairs with a 35-mm camera has been field tested under rigorous field conditions. It is workable and can easily be performed by someone with the basic skills necessary to operate a camera and theodolite. Stereopairs analyzed using a parallax correction graph provided the desired accuracy to within one foot for the glacier photography at distances up to 110 feet.

The system discussed can be applied in a variety of data collection problems where terrestrial photogrammetry is applicable and a high degree of accuracy is not required. Cost will be relatively low. In applications where the object space is not dangerous (i.e., non-glacial areas) further simplification of the targeting system could be carried out. With a calibrated camera, such simplification may result in a system that a lay person could employ.

ACKNOWLEDGMENTS

The following persons and organization deserve special thanks for either their valuable time or funding: Prof. Paul R. Wolf, Prof. James Clapp, Prof. James Scherz, Mrs. Sue Brunsell, The Canadian Exploration Group, Expedition Training Institute, Explorers Club, and the National Science Foundation.

REFERENCES

Wolf, P. R., 1974. *Elements of Photogrammetry*, McGraw-Hill, New York.

Wolf, P. R., and S. A. Loomer, 1975. Calibration of a Non-Metric Camera, *Proceedings, Symposium on Close Range Photogrammetry*, Champaign, Illinois.

Wolf, P. R., and R. A. Pearsall, 1976. The Kern PG-2 as a Monocomparator, *Photogrammetric Engineering and Remote Sensing*, Vol. 42, No. 10, pp. 1253-1259.

(Received 3 October 1980; revised and accepted 15 March 1982)

Forthcoming Articles

O. O. Ayeni, Optimum Sampling for Digital Terrain Models: A Trend Towards Automation.
O. O. Ayeni, Phototriangulation: A Review and Bibliography.
Gérard Begni, Selection of the Optimum Spectral Bands for the SPOT Satellite.
R. G. Best, *R. Fowler*, *D. Hause*, and *M. Wehde*, Aerial Thermal Infrared Census of Canada Geese in South Dakota.
P. D. Carman, Aerial Camera Vibration.
Alden P. Colvocoresses, An Automated Mapping Satellite System (Mapsat).
David O. Cook, *Gary R. Davis*, *Ronald A. Franklin*, and *Timothy L. Flynn*, Use of Aerial Photography with Loran C Positioning to Map Offshore Surface Currents.
Thomas L. Erb and *Warren R. Philipson*, Producing Stereo Teaching Aids from Aerial Photographs.
Barry M. Evans, Aerial Photographic Analysis of Septic System Performance.
R. D. Graetz and *M. R. Gentle*, The Relationships between Reflectance in the Landsat Wavebands and the Composition of an Australian Semi-Arid Shrub Rangeland.
G. Ladouceur, *P. Trotier*, and *R. Allard*, Zeiss Stereotop Modified into an Analytical Stereoplotter.
L. Daniel Maxim and *Leigh Harrington*, To Mix or Match: On Choosing Matched Samples in Comparative Aerial Surveys.
James M. Palmer, Field Standards of Reflectance.
John C. Price, Satellite Orbital Dynamics and Observation Strategies in Support of Agricultural Applications.
A. Prieto, *J. Bescós*, and *J. Santamaria*, Spatial Frequency Pseudocolor Filters.
John P. Snyder, Geometry of a Mapping Satellite.
J. C. Trinder, The Effects of Photographic Noise on Pointing Precision, Detection, and Recognition.
Manmohan M. Trivedi, *Clair L. Wyatt*, and *David R. Anderson*, A Multispectral Approach to Remote Detection of Deer.